Journal of Alloys and Compounds 694 (2017) 40–45

Contents lists available at ScienceDirect

Journal of Alloys and Compounds

journal homepage: http://www.elsevier.com/locate/jalcom

Structure, Raman spectra, far-infrared spectra and microwave dielectric properties of temperature independent $CeVO_4$–TiO_2 composite ceramics

Wen-Bo Li [a], Di Zhou [a, b, c, *], Dan Guo [a], Li-Xia Pang [c, d], Guo-Hua Chen [e], Ze-Ming Qi [f], Qiu-Ping Wang [g], Han-Chen Liu [g]

[a] Electronic Materials Research Laboratory, Key Laboratory of the Ministry of Education & International Center for Dielectric Research, Xi'an Jiaotong University, Xi'an 710049, Shaanxi, China
[b] Xi'an Jiaotong University Suzhou Academy, Suzhou 215123, Jiangsu, China
[c] Department of Materials Science and Engineering, University of Sheffield, S1 3JD, UK
[d] Micro-optoelectronic Systems Laboratories, Xi'an Technological University, Xi'an 710032, Shaanxi, China
[e] Guangxi Key Laboratory of Information Materials, Guilin University of Electronic Technology, Guilin 541004, China
[f] National Synchrotron Radiation Laboratory, University of Science and Technology of China, Anhui, 230029, Hefei, China
[g] School of Science, Xi'an Polytechnic University, Xi'an 710048, China

ARTICLE INFO

Article history:
Received 21 August 2016
Received in revised form
21 September 2016
Accepted 30 September 2016
Available online 1 October 2016

Keywords:
Sinteringo
Ceramicso
Microwave dielectric propertieso
TiO_2o

ABSTRACT

A series of temperature-stable microwave dielectric $(1-x)CeVO_4$-$xTiO_2$ ($0.0 \leq x \leq 0.4$) ceramics were prepared by using solid-state reaction method. All the samples could be sintered well at 1025 °C-1150 °C for 2 h. X-ray diffraction (XRD) and energy-dispersive spectroscopy (EDS) analysis revealed that rutile TiO_2 and tetragonal $CeVO_4$ phases coexisted in the ceramics. Raman spectroscopy and infrared spectra were used to study relationship between structure and microwave dielectric properties. $(1-x)CeVO_4$-$xTiO_2$ ceramics with $0.15 \leq x \leq 0.20$ sintered at 1100 °C for 2 h exhibited good microwave dielectric properties with relative permittivities (ε_r) ~ 11.2–14.2, quality factor ($Q \times f$) values ~ 7950–22,100 GHz (at 9.2–9.5 GHz), and near zero temperature coefficient of resonant frequencies (τ_f) ~ −1.2 to +2.8 ppm/°C. The infrared spectra study showed that the external vibrations of $CeVO_4$ had the most remarkable effects on the dielectric constant. All these results indicate that this system is a good candidate for microwave devices applications in the future.

1. Introduction

In the past few decades, with the rapid development of wireless communication, microwave dielectric materials have been widely studied for practical application in Global Position System (GPS), Wireless Local Area Network (WLAN) technology, and other key components in microwave communication systems [1–4]. Microwave dielectric ceramics with high permittivities (ε_r), high quality factor ($Q \times f$), and near zero temperature coefficient of resonant frequency (τ_f) are indispensable for microwave (MW) applications [5–7]. Many works have been done to search for novel microwave dielectric ceramics with promising microwave dielectric properties [8–10].

More recently, some V_2O_5-rich ceramics have attracted much attention because of their low sintering temperatures and promising microwave dielectric properties. Cerium vanadate, $CeVO_4$, is a rare earth orthovanadate with zircon-type tetragonal structure and it can be used as oxidation catalyst, photocatalyst, gas sensor material, and pigment [11–13]. As technologically important material, $CeVO_4$ ceramic was reported to be sintered at 950 °C with a permittivity value of ~12.3, a $Q \times f$ value of ~41,500 GHz, and a τ_f value of ~ −34.4 ppm/°C [14]. However, the negative τ_f values may limit its application in microwave devices. As well know, there are two methods to adjust τ_f values of microwave dielectric ceramics to near zero. The first one is to form solid solution and the other method is to design composite materials with components possessing opposite τ_f values. Our previous works pointed that

* Corresponding author. Electronic Materials Research Laboratory, Key Laboratory of the Ministry of Education & International Center for Dielectric Research, Xi'an Jiaotong University, Xi'an 710049, Shaanxi, China.
E-mail address: zhoudi1220@gmail.com (D. Zhou).

http://dx.doi.org/10.1016/j.jallcom.2016.09.327
0925-8388/

composite ceramics route is a good method to achieve temperature stable microwave dielectric ceramics [15,16]. As a well-known material with high ε_r (105), high quality factor ($Q \times f = 46{,}000$ GHz at 5 GHz), and large positive τ_f value (+465 ppm/°C), rutile TiO_2 is a useful material to compensate negative τ_f values in composite ceramics [17]. *Guo* et al. studied the microwave dielectric properties of the $AMoO_4$-TiO_2 (A = Ca, Sr, Ba) ceramics and found that all the composite ceramics exhibit near-zero τ_f value and high quality factor ($Q \times f = 40{,}700$–$72{,}050$ GHz) [18]. Furthermore, the $(1-x)LiMVO_4$–$xTiO_2$ (M = Mg, Zn; x = 0.20–0.45) ceramics with relative permittivities of 9.7–20.1, $Q \times f$ values of 20,100–39,200 GHz and near zero τ_f values of −20-5 ppm/°C were reported in our previous work [19]. In the present work, the $(1-x)CeVO_4$-$xTiO_2$ ($0.0 \le x \le 0.4$) composite ceramics were synthesized by using solid state reaction method. Sintering behavior, phase composition, microstructures, microwave dielectric properties, and relation between structure and microwave dielectric properties of the $CeVO_4$–TiO_2 ceramics were studied in detail.

2. Experimental procedure

$(1-x)CeVO_4$-$xTiO_2$ ($0.0 \le x \le 0.4$) ceramics were prepared by using traditional solid state reaction method as described previously [4,8]. The mixture was first calcined in air at 600 °C-800 °C for 4 h. After re-milling for 5 h, powders were pressed into cylinders with polyvinyl alcohol addition as binder. Finally samples were sintered at 1025 °C–1150 °C for 2 h (3 °C/min).

The phase compositions and crystalline structures of samples were investigated by using X-ray diffraction (XRD) with Cu Kα radiation (Rigaku D/MAX-2400 X-ray diffractometer, Tokyo, Japan) at a scanning rate of $0.02°s^{-1}$ in a 2θ range of 10°-70°. Microstructures of the sintered ceramic were characterized with scanning electron microscopy (SEM) (SEM; Quanta 250 F, FEI) and the chemical constitution was examined by energy-dispersive spectrometer. The Raman spectra were recorded at room temperature using a Raman spectrometer (inVia, Renishaw, England) excited with an Ar^+ laser (514.5 nm). The room temperature infrared reflectivity spectra were measured using a Bruker IFS 66v FTIR spectrometer on Infrared beamline station (U4) at National Synchrotron Radiation Lab. (NSRL), China. Microwave dielectric behaviors were measured with the $TE_{01\delta}$ shielded cavity method with a network analyzer (8720 ES, Agilent, Palo Alto, CA) and a temperature chamber (Delta 9023, Delta Design, Powa CA) in the temperature range of 25 °C-85 °C. Temperature coefficient of resonant frequency (TCF or τ_f value) was calculated with the following formula:

$$TCF = \frac{f_{85} - f_{25}}{f_{25}(85-25)} \times 10^6 (ppm/°C) \quad (1)$$

where f_{85} and f_{25} are the $TE_{01\delta}$ resonant frequencies at 85 °C and 25 °C, respectively.

3. Results and discussion

Fig. 1 shows XRD patterns of the $(1-x)CeVO_4$-$xTiO_2$ ($0.0 \le x \le 0.4$) ceramic samples sintered at different temperatures. It is seen that all diffraction peaks could be indexed as both $CeVO_4$ and rutile TiO_2 phases ($CeVO_4$ with PDF: 32-0574 and rutile TiO_2 with PDF: 38-1332). From the XRD results, it is seen that when x value increased, the diffraction intensities of TiO_2 increased gradually and no secondary phases can be detected, which further confirmed the chemical compatibility. Fig. 1b illustrates the backscattered electron images (BEI) and EDS analysis of as-fired surfaces of $0.8CeVO_4$-$0.2TiO_2$ compounds sintered at 1100 °C/2 h. It can be

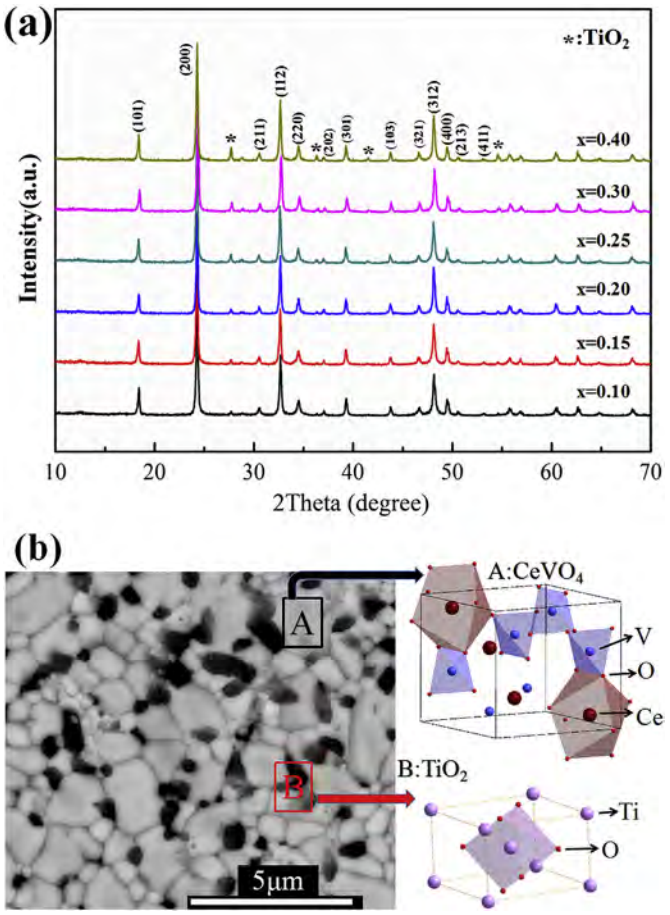

Fig. 1. Structural characterization of $(1-x)CeVO_4$-$xTiO_2$ ($0.1 \le x \le 0.4$). (a) XRD pattern of the sample. (b) Backscattered electron micrographs of the $CeVO_4$–TiO_2.

seen that there are two types of grains, one with dark-color and the other with light-color, and they are marked as "A" and "B", respectively. EDS analysis is employed to identify the chemical compositions of different grains. According to EDS analysis (not shown here), the small grains (0.5–1 μm) marked with "A" belong to TiO_2 phase and the large grains (4–7 μm) marked with "B" belong to $CeVO_4$ phase as shown in Fig. 1b. All the results indicate that the $CeVO_4$ could coexist with TiO_2 phase during sintering process and a stable two-phase composite system $CeVO_4$–TiO_2 was established. Fig. 1b shows the schematic crystal structure of $CeVO_4$ and rutile TiO_2. As sketched in Fig. 1c, the tetragonal $CeVO_4$ ceramics with a zircon structure [space group $I4_1/amd$ (No. 141)], which is composed of CeO_8 dodecahedra and VO_4 tetrahedra. Rutile TiO_2 has a tetragonal structure with space-group symmetry $P42/mnm$ (No. 136). Rutile TiO_2 is composed of TiO_6 octahedra with comparatively simple structure [20].

Fig. 2 shows SEM images of the $(1-x)CeVO_4$–$xTiO_2$ ($0.1 \le x \le 0.4$) ceramics sintered at 1100 °C/2 h. The $CeVO_4$–TiO_2 ceramics exhibit dense microstructures and average grain size of 2–5 μm. It can be observed that the grain size of the ceramics is very sensitive to TiO_2 contents. For $0.1 \le x \le 0.25$ samples, it can be noticed that there are two kinds of grains with different morphology. The large grains become much larger and small grains become much smaller as the TiO_2 contents increases, as shown in Fig. 2a-(d). At the same time, small grains fill up the gap of large grains to make a denser microstructure.

Fig. 3a and b presents the microwave dielectric properties of the $(1-x)CeVO_4$–$xTiO_2$ ($0.0 \le x \le 0.4$) ceramics as a function of x

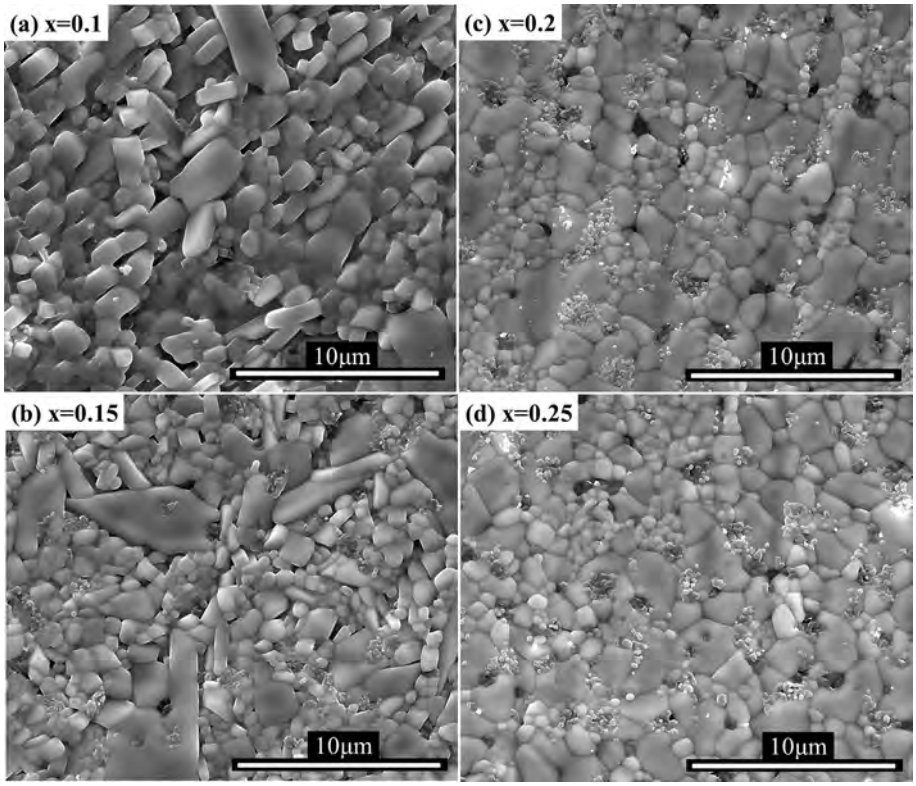

Fig. 2. SEM images of surfaces of $(1-x)CeVO_4$-$xTiO_2$ ($0.1 \le x \le 0.4$) sintered at 1100 °C/2 h: (a) x = 0.10; (b) x = 0.15; (c) x = 0.20; (d) x = 0.25.

values and sintering temperature. As seen from Fig. 3a, the ε_r and τ_f of the $(1-x)CeVO_4$-$xTiO_2$ ($0.0 \le x \le 0.4$) ceramics increased linearly with x value. As we know, ε_r of composite is determined by the permittivity, volume fraction and grain boundaries of the constituents. There are a lot of models to predict the effective permittivity of composite. The Lichtenecker formula is an empirical rule, which is also applicable to composite materials aligned randomly [21,22]:

$$\lg\varepsilon_r = V_1 \times \lg\varepsilon_{r1} + V_2 \times \lg\varepsilon_{r2} \quad (2)$$

where ε_{r1} and ε_{r2} are ε_r of $CeVO_4$ and TiO_2, V_1 and V_2 represent the volume fractions of $CeVO_4$ and TiO_2, respectively. Fig. 3a shows that the permittivity of the $(1-x)CeVO_4$–$xTiO_2$ ($0.0 \le x \le 0.4$) ceramics increases from around 11.7 to around 14.2 when the volume fraction of TiO_2 increased from 0 to 0.4. It is believed that ε_r is significantly affected the density and secondary phases in composite. The dielectric permittivity of rutile TiO_2 ($\varepsilon_r = 105$) is much larger than that of the $CeVO_4$ ceramic ($\varepsilon_r = 12.3$). Although the measured ε_r is different from the calculated one, they are very close to each other. It generally accords with the logarithmic rule. The theoretical τ_f values of the mixture are predicted by the semi-empirical linear model:

$$\tau_f = V_1 \times \tau_{f1} + V_2 \times \tau_{f2} \quad (3)$$

where τ_{f1} and τ_{f2} are the τ_f values of $CeVO_4$ and TiO_2, V_1 and V_2 represent the volume fractions of $CeVO_4$ and TiO_2, respectively. Compared with the previous reports [14], the measured τ_f values of pure $CeVO_4$ are a little lower and the measured τ_f value of rutile TiO_2 is a little larger, which may be caused by the different processing parameters. τ_f values of the $(1-x)CeVO_4$-$xTiO_2$ ($0.0 \le x \le 0.4$) ceramics agree well with equation (3). As shown in Fig. 3a, Q × f values of show a downtrend with x. This is probably due to the large amount of grain boundaries created by large difference of two different grains.

Microwave dielectric properties of the $(1-x)CeVO_4$-$xTiO_2$ ($0.15 \le x \le 0.2$) ceramics as a function of sintering temperature are shown in Fig. 3b. The ε_r of the $(1-x)CeVO_4$-$xTiO_2$ ($0.15 \le x \le 0.2$) ceramics increased first to saturated value and then decreased as the sintering temperature is increased from 1025 °C to 1150 °C. The variation of Q × f value versus sintering temperature presented similar behavior to that of ε_r. Generally, the Q × f value is affected by intrinsic parameters, such as structural characteristics and extrinsic parameters, such as porosity, secondary phases, lattice defects, impurity and microstructural characteristics [23–25]. As shown in Fig. 3b, high performance of microwave dielectric properties can be obtained in $0.85CeVO_4$-$0.15TiO_2$ ceramics sintered at 1100 °C for 2 h, with a ε_r ~13.7, a Q × f ~22,100 GHz (at 9.5 GHz) and a $\tau_f \sim -1.2$ ppm/°C. The $0.8CeVO_4$-$0.2TiO_2$ ceramics can be sintered well at 1150 °C for 2 h, with a ε_r of 13.9, a Q × f value of 19,600 GHz (at 9.46 GHz), a τ_f value of +2.8 ppm/°C.

To give an insight into the relationships between structures and dielectric properties of $CeVO_4$–TiO_2 ceramics, Raman spectroscopy and infrared spectra are applied to complement. The results are discussed by group theory. Previous theoretical analysis indicated that there are 12 Raman active modes ($2A_{1g} + 4B_{1g} + B_{2g} + 5E_g$) for the zircon-type structure $CeVO_4$ with the space group $I4_1/and$ (D^{19}_{4h}) and 5 Raman active modes ($1A_{1g} + 1B_{1g} + 1B_{2g} + 2E_g$) for the rutile structure TiO_2 with the space group $P42/mnm$ [26–28]. The letters A and B represent non degenerate modes whereas E denotes doubly degenerate mode. The subscripts g indicates even parity of inversion in centrosymmetric crystals [28].

Fig. 4 illustrates the room-temperature Raman spectra of $(1-x)CeVO_4$-$xTiO_2$ ($0.1 \le x \le 0.3$) ceramics in the range of 100–1000 cm^{-1}. In the Raman spectrum of $CeVO_4$–TiO_2 ceramics, five Raman modes of $CeVO_4$ are observed at 261, 372, 461, 771, and

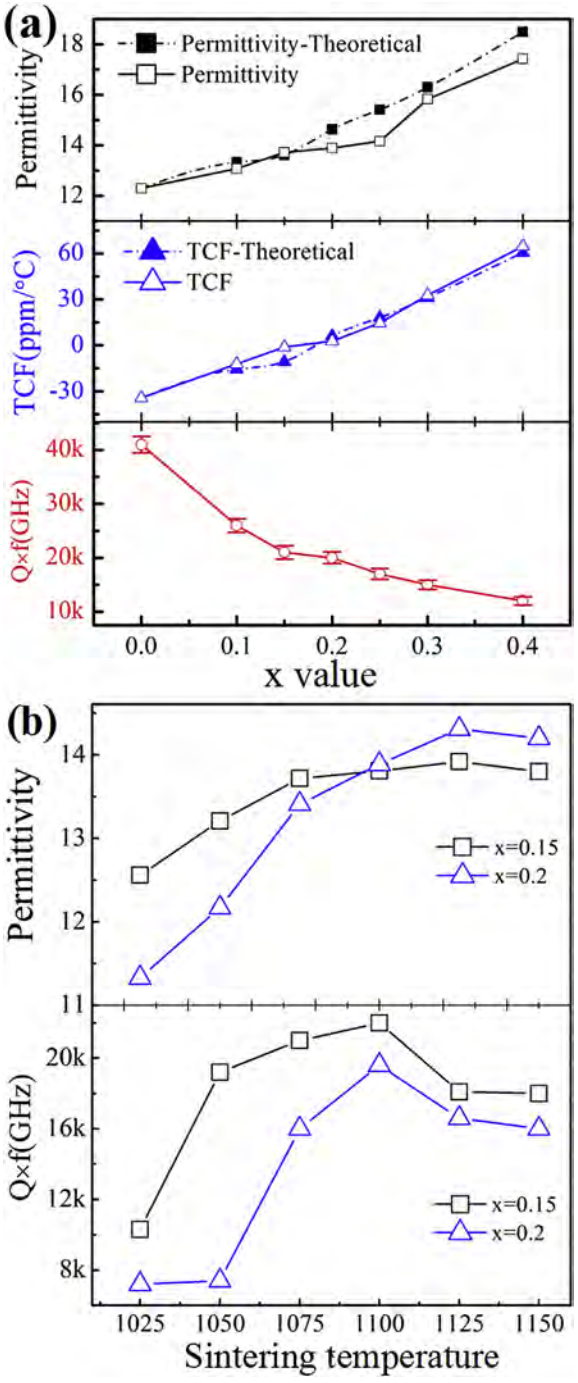

Fig. 3. Microwave dielectric properties of the $(1-x)CeVO_4$–$xTiO_2$ as a function of volume fraction of TiO_2 (a) and sintering temperature (b).

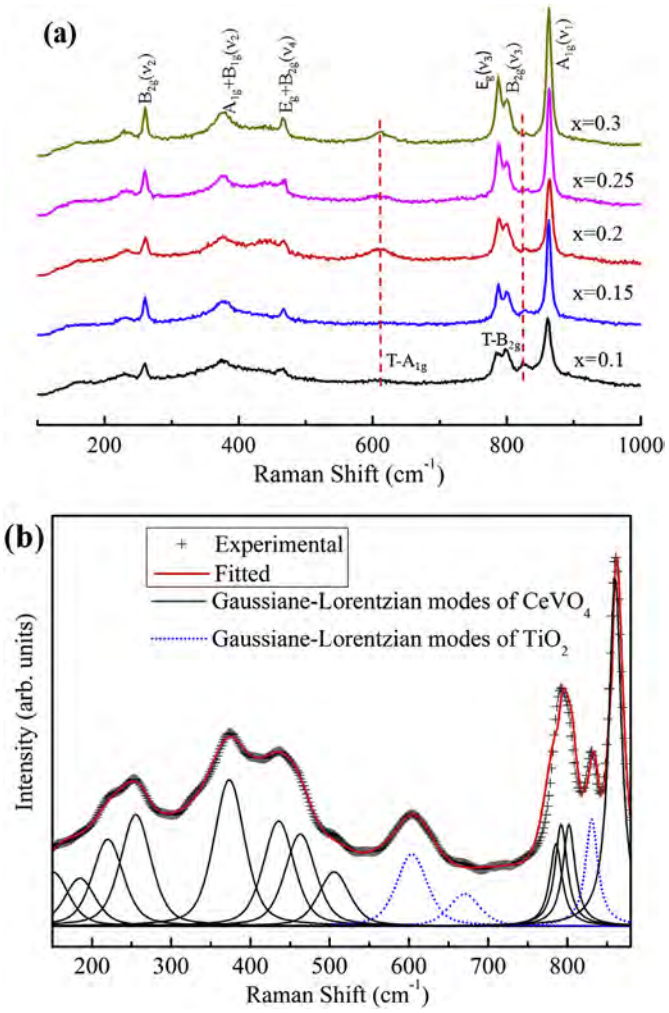

Fig. 4. Raman spectra of $(1-x)CeVO_4$–$xTiO_2$ ($0.15 \leq x \leq 0.3$) ceramics. The solid red circles are the fitted data and the dashed line indicates the Gaussian–Lorentzian mode fitting. Black and blue dashed lines are assigned to $CeVO_4$ and TiO_2, respectively. (For interpretation of the references to colour in this figure legend, the reader is referred to the web version of this article.)

847 cm^{-1}. The 261-cm^{-1} modes is assigned as B_{2g} deformation (ν_2), 372-cm^{-1} modes is assigned as $A_{1g} + B_{1g}$ deformation (ν_2), 461 cm^{-1} modes is assigned as $E_g + B_{2g}$ deformation (ν_4), 771 cm^{-1} and 847 cm^{-1} are assigned as E_g asymmetric stretch (ν_3) and A_{1g} symmetric stretch (ν_1), respectively [29–31]. The typical bands for TiO_2 were located at 220, 430, 610, and 830 cm^{-1} The Raman band at 830 cm^{-1} was assigned to B_{2g} mode, at 610 cm^{-1} to the A_{1g} mode, at 430 and 220 cm^{-1} to E_g mode and B_{1g} respectively. When x value increases, there are significant changes in the intensity of all the peaks of TiO_2, especially the characteristic band of Rutile TiO_2 phase at 610 cm^{-1}.

In order to observe the Raman spectral changes clearly, the Raman spectra have been fitted using the mixture of Gaussian-Lorentzian distribution peak profile called Pseudo Voigt peak shape function. Fig. 4b shows representative Raman spectra of $0.85CeVO_4$-$0.15TiO_2$ de-convoluted into 15 peaks with varying intensity, wave number and FWHM. As seen from Fig. 4b, blue marked modes are assigned to TiO_2 and the peak position of modes at 261, 372, 461, 514, 771, and 847 cm^{-1} are assigned to $CeVO_4$.

Fig. 5 presents the IR reflectivity spectra and complex dielectric spectra of $0.85CeVO_4$-$0.15TiO_2$ ceramic ranging from 50 to 1000 cm^{-1}. It is seen that the infrared spectra were fitted by 11 resonant modes corresponding with the infrared reflectivity peaks. The phonon parameters obtained from the fitting of the infrared reflectivity spectra of the $0.85CeVO_4$–$0.15TiO_2$ ceramic are shown in Table 1. Among all the fitted modes, 3 vibration modes at 180–190 cm^{-1}, 385–410 cm^{-1}, and 500–620 cm^{-1} correspond to TiO_2 and the others belong to $CeVO_4$. There spectra have been analyzed by using the classical harmonic oscillator model based on the standard Lorentzian formula [Eq (4)] and the Fresnel formula [Eq (5)]:

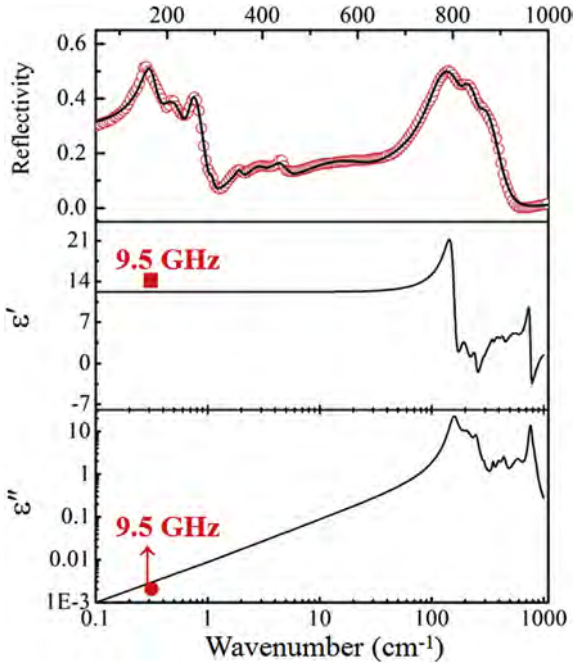

Fig. 5. Measured and calculated infrared reflectivity spectra and complex dielectric spectra of the $0.85CeVO_4$–$0.15TiO_2$ ceramic (solid line for fitting values and hollow symbol for measured values, circles are experimental at microwave region, and solid lines represent the fit of IR spectra).

Table 1
Phonon parameters obtained from the fitting of the infrared reflectivity spectra of $0.85CeVO_4$–$0.15TiO_2$ ceramic.

Mode	ω_{oj}	ω_{pj}	γ_j	$\Delta\varepsilon_j$
1	159.57	316.56	31.258	6.94
2	208.20	316.52	61.309	4.31
3	249.87	178.60	26.266	0.51
4	292.93	30.29	8.340	0.011
5	353.95	77.48	18.58	0.048
6	396.54	135.68	43.305	0.117
7	441.95	179.29	44.465	0.165
8	587.55	411.51	159.46	0.491
9	762.84	761.90	56.694	0.998
10	821.07	171.68	35.775	0.044
11	859.92	104.30	30.728	0.015

x = 0.15: $\varepsilon_\infty = 3.51$ and $\varepsilon_0 = 14.2$.

$$\varepsilon^*(\omega) = \varepsilon_\infty + \sum_{j=1}^{n} \frac{\omega_{pj}^2}{\omega_{oj}^2 - \omega^2 - j\gamma_j\omega} \tag{4}$$

$$R(\omega) = \left| \frac{1 - \sqrt{\varepsilon^*(\omega)}}{1 + \sqrt{\varepsilon^*(\omega)}} \right|^2 \tag{5}$$

where $\varepsilon^*(\omega)$ is complex dielectric function; ε_∞ is the dielectric constant caused by the electronic polarization at high frequencies; ω_{pj}, ω_{oj} and γ_j are the plasma frequency, the transverse frequency, and damping factor of the j-th Lorentz oscillator, respectively; n is the number of transverse phonon modes; $R(\omega)$ is the IR reflectivity.

Fig. 5 also shows the calculated permittivity $\varepsilon'(\omega)$ and loss $\varepsilon''(\omega)$ obtained from the fits of the infrared reflectivity together with the experimental microwave data. It is seen that the calculated permittivities are a little smaller than the measured ones in the microwave range. It can be concluded that some extrinsic contributions, especially the grain size and pores, increase the microwave losses. Meanwhile, all the calculated dielectric permittivity and dielectric loss values are almost equal to the measured ones using $TE_{01\delta}$ method. Therefore, it can be concluded that majority of the dielectric contribution for $CeVO_4$–TiO_2 system at microwave region was attributed to the absorptions of phonon oscillation at infrared region and very little contribution from defect phonon scattering. Phonon parameters obtained from the fitting of the infrared reflectivity spectra of the $0.85CeVO_4$-$0.15TiO_2$ ceramics are given in Table 1. For the $CeVO_4$–TiO_2 samples, the values of $\Delta\varepsilon_j$ represent the mode makes the contribution to the permittivity. Hence, it can be calculated from Table 1 that the external vibrations of $CeVO_4$ and TiO_2 make different contribution to $CeVO_4$–TiO_2 ceramics and the external vibrations of $CeVO_4$ have the most remarkable effects on the dielectric constant.

4. Conclusion

In the present work, the temperature stable $(1-x)CeVO_4$–$xTiO_2$ ($0.0 \le x \le 0.4$) ceramics were obtained by the solid-state reaction method. According to XRD and EDS analysis, there are two phases in the ceramics and the $CeVO_4$ phase could coexist with rutile TiO_2 phase at their sintering temperatures. With the increase of TiO_2 content, the ε_r increases, and the τ_f value changes from negative into positive. High performance of microwave dielectric properties can be obtained in the $(1 - x)CeVO_4$–$xTiO_2$ ($0.15 \le x \le 0.20$) ceramics with ε_r of 11.2–14.2, $Q \times f$ values from 7950 to 22,100 GHz, and τ_f values from −1.2 ppm/°C to +2.8 ppm/°C.

Acknowledgements

This work was supported by the Young Star Project of Science and Technology of Shaanxi Province (2016YFXX0029), the Fundamental Research Funds for the Central University, Guangxi Key Laboratory of Information Materials (Guilin University of Electronic Technology), P.R. China (Project No. 161004-K), and the 111 Project of China (B14040). The authors would like to thank the administrators in IR beamline workstation (BL01B) of National Synchrotron Radiation Laboratory (NSRL) for their help in the IR measurement and fitting. SEM work was done at the International Center for Dielectric Research (ICDR), Xi'an Jiaotong University, Xi'an, China and the authors thank Ms. Yan-Zhu Dai for her help in using SEM.

References

[1] M.T. Sebastian, H. Jantunen, Low loss dielectric materials for LTCC applications: a review, Int. Mater. Rev. 53 (2008) 57–90.
[2] I.M. Reaney, D. Iddles, Microwave dielectric ceramics for resonators and filters in mobile phone networks, J. Am. Ceram. Soc. 89 (2006) 2063–2072.
[3] A.K. Axelsson, N.M. Alford, Bismuth titanates candidates for high permittivity LTCC, J. Eur. Ceram. Soc. 26 (2006) 1933–1936.
[4] D. Zhou, L.X. Pang, J. Guo, Z.M. Qi, T. Shao, Q.P. Wang, H.D. Xie, X. Yao, C.A. Randall, Influence of Ce substitution for Bi in $BiVO_4$ and the impact on the phase evolution and microwave dielectric properties, Inorg. Chem. 53 (2014) 1048–1055.
[5] C.L. Huang, W.R. Yang, P.C. Yu, High-Q microwave dielectrics in low-temperature sintered $(Zn_{1-x}Ni_x)_3Nb_2O_8$ ceramics, J. Eur. Ceram. Soc. 34 (2014) 277–284.
[6] Y.P. Guo, H. Ohsato, K. Kakimoto, Characterization and dielectric behavior of willemite and TiO_2-doped willemite ceramics at millimeter-wave frequency, J. Eur. Ceram. Soc. 26 (2006) 1827–1830.
[7] D. Zhou, H. Wang, L.X. Pang, C.A. Randall, X. Yao, Bi_2O_3–MoO_3 binary system: an Alternative ultralow sintering temperature microwave dielectric, J. Am. Ceram. Soc. 92 (2009) 2242–2246.
[8] L.X. Pang, D. Zhou, W.G. Liu, Low-temperature sintering and microwave dielectric properties of $CaMoO_4$-based temperature stable LTCC material, J. Am. Ceram. Soc. 97 (2014) 2032–2034.
[9] D. Zhou, D. Guo, W.B. Li, L.X. Pang, X. Yao, D.W. Wang, I.M. Reaney, Novel temperature stable high-ε_r microwave dielectrics in the Bi_2O_3-TiO_2-V_2O_5 system, J. Mater. Chem. C 4 (2016) 5357–5362.
[10] G.K. Choi, J.R. Kim, S.H. Yoon, K.S. Hong, Microwave dielectric properties of

scheelite (A = Ca, Sr, Ba) and wolframite (A =Mg, Zn, Mn) $AMoO_4$ compounds, J. Eur. Ceram. Soc. 27 (2007) 3063–3067.
[11] Y.K. Kim, H.M. Jang, Lattice contraction and cation ordering of $ZrTiO_4$ in the normal-to-incommensurate phase transition, J. Appl. Phys. 89 (2001) 6349–6355.
[12] P.F. Chen, Q. Wu, L. Zhang, W.F. Yao, Facile immobilization of $LnVO_4$ (Ln = Ce, Nd, Gd) on silica fiber via a combined alcohol-thermal and carbon nanofibers template route, Catal. Commun. 66 (2015) 6–9.
[13] M.V. Boscoa, M.A. Banares, M.V. Martínez-Huerta, A.L. Bonivardi, S.E. Collins, In situ FTIR and Raman study on the distribution and reactivity of surface vanadia species in V_2O_5/CeO_2 catalysts, J. Mol. Catal. A-Chem. 408 (2015) 75–84.
[14] J. Hou, H.H. Huang, Z.Z. Han, H.B. Pan, The role of oxygen adsorption and gas sensing mechanism for cerium vanadate ($CeVO_4$) nanorods, RSC Adv. 6 (2016) 14552–14558.
[15] Y. Wang, R.Z. Zuo, C. Zhang, J. Zhang, T.W. Zhang, Low-temperature-fired $ReVO_4$ (Re = La, Ce) microwave dielectric ceramics, J. Am. Ceram. Soc. 98 (2015) 1–4.
[16] D. Zhou, W.B. Li, H.H. Xi, L.X. Pang, G.S. Pang, Phase composition, crystal structure, infrared reflectivity and microwave dielectric properties of temperature stable composite ceramics (scheelite and zircon-type) in $BiVO_4$–YVO_4 system, J. Mater. Chem. C 3 (2015) 2582–2588.
[17] W.B. Li, D. Zhou, H.H. Xi, L.X. Pang, X. Yao, Structure, infrared reflectivity and microwave dielectric properties of $(Na_{0.5}La_{0.5})MoO_4$–$(Na_{0.5}Bi_{0.5})MoO_4$ ceramics, J. Am. Ceram. Soc. 99 (2016) 2083–2088.
[18] K. Fukuda, R. Kitoh, I. Awai, Microwave characteristics of TiO_2-Bi_2O_3 dielectric resonator, Jpn. J. Appl. Phys. 32 (1993) 4584–4588.
[19] J. Guo, D. Zhou, L. Wang, H. Wang, T. Shao, Z.M. Qi, X. Yao, Infrared spectra, Raman spectra, microwave dielectric properties and simulation for effective permittivity of temperature stable ceramics $AMoO_4$–TiO_2 (A = Ca, Sr), Dalton Trans. 42 (2013) 1483–1491.
[20] W.B. Li, H.H. Xi, D. Zhou, Microwave dielectric properties of $LiMVO_4$ (M = Mg, Zn) ceramics with low sintering temperatures, Ceram. Int. 41 (2015) 9063–9068.
[21] Z. Chen, H. Jia, K. Sharafudeen, W.B. Dai, Y.B. Liu, G.Q. Dong, J.R. Qiu, Up-conversion luminescence from single vanadate through blackbody radiation harvesting broadband near-infrared photons for photovoltaic cells, J. Alloy. Compd. 663 (2016) 204–210.
[22] A.N. Norris, P. Sheng, A.J. Callegari, Effective-medium theories for two-phase dielectric media, J. Appl. Phys. 57 (1985) 1990–1996.
[23] P.N. Sen, C. Scala, M.H. Cohen, A self-similar model for sedimentary rocks with application to the dielectric constant of fused glass beads, Geophysics 46 (1981) 781–795.
[24] N.M. Alford, J. Breeze, X. Wang, S.J. Penn, S. Dalla, S.J. Webb, N. Ljepojevic, X. Aupi, Dielectric loss of oxide single crystals and poly-crystalline Analogues from 10 to 320 K, J. Eur. Ceram. Soc. 21 (2001) 2605–2611.
[25] S.J. Penn, N. Alford, A. Templeton, X. Wang, M. Xu, M. Reece, K. Schrapel, Effect of porosity and grain size on the microwave dielectric properties of sintered Alumina, J. Am. Ceram. Soc. 80 (1997) 1885–1888.
[26] L.X. Pang, H. Liu, D. Zhou, G.B. Sun, W.G. Qin, W.G. Liu, Microwave dielectric ceramic with intrinsic low firing temperature: $BaLa_2(MoO_4)_4$, Mater. Lett. 72 (2012) 128–130.
[27] P. Dawson, M.M. Hargreave, G.R. Wilkinson, The vibrational spectrum of zircon ($ZrSiO_4$), J. Phys. C. Solid State Phys. 4 (1971) 240–256.
[28] A.A. Kaminskii, J. Zhang, O. Lux, H. Rhee, H.J. Eichler, D.V. Tang, H.H. Yu, H.J. Zhang, J. Wang, H. Yoneda, A. Shirakawa, Stimulated Raman scattering spectroscopy of $Y_{0.4}Gd_{0.6}VO_4$ crystals with partly disordered zircon-type structure-observation of new $\chi^{(3)}$-nonlinear optical interactions, Laser Phys. Lett. 11 (2014) 125808.
[29] W.G. Spitzer, R.C. Miller, D.A. Kleinman, L.E. Howarth, Far infrared dielectric dispersion in $BaTiO_3$, $SrTiO_3$, and TiO_2, Phys. Rev. 126 (1962) 1710–1721.
[30] C.C. Santos, E.N. Silva, A.P. Ayala, I. Guedes, P.S. Pizani, C.K. Loong, L.A. Boatner, Raman investigations of rare earth orthovanadates, J. Appl. Phys. 101 (2007) 053511.
[31] U.O. Krasovec, B. Orel, A. Surca, N. Bukovec, R. Reisfeld, Structural and spectroelectrochemical investigations of tetragonal $CeVO_4$ and Ce/V-oxide sol-gel derived ion-storage films, Solid State Ion. 118 (1999) 195–214.